Equatorward Propagation of Coupled Air–Sea Disturbances with Application to the Annual Cycle of the Eastern Tropical Pacific

ZHENGYU LIU

Department of Atmospheric and Oceanic Sciences, University of Wisconsin-Madison, Madison, Wisconsin

SHANGPING XIE*

Program in Atmospheric and Oceanic Sciences, Princeton University, Princeton, New Jersey

(Manuscript received 23 August 1993, in final form 12 April 1994)

ABSTRACT

A simple coupled ocean–atmospheric boundary layer model is used to study the annual variability in the eastern tropical Pacific. The air–sea coupling, particularly the feedback of the total wind speed effect on evaporation and wind mixing entrainment, produces a rapid equatorward and westward propagation of annual disturbances. For reasonable parameters, both amplitude and phase of the annual disturbance can be reproduced fairly well over most of the Tropics. It is then suggested that a substantial part of equatorial annual variability may come from the extratropics (say beyond 15°) due to the propagation of coupled waves.

1. Introduction

One striking feature of the eastern equatorial Pacific is a strong annual cycle in the sea surface temperature (SST) field despite the dominant semiannual solar radiation component there. In March, the SST reaches its maximum with a weak southward surface wind component; in September, the SST achieves its minimum with a strong northward surface wind component (Horel 1982). Figure 1 presents the amplitude and phase of the annual harmonic SST in the tropical Pacific analyzed from COADS (Coupled Ocean–Atmosphere Data Set) data (Koeberle and S. G. H. Philander 1992 personal communication). The amplitude in Fig. 1a shows that the maximum annual SST variability exceeds 3.5°C along the South American coast at about 15°S. The variability diminishes westward to 1°C at 60 degrees away from the coast along the equator. The phase in Fig. 1b further shows that this annual signal starts from the eastern boundary to the south of the equator and propagates northwestward. This annual signal is in sharp contrast to that in the western Pacific where the SST variability is weak and a semiannual component is dominant.

So far, the physical mechanism for the annual cycle of the coupled ocean–atmosphere system in the equator is not well understood. Unlike the ENSO phenomenon, which lacks an external forcing at its frequency, the annual forcing is strong in the extratropics. Indeed, the annual solar radiation increases rapidly away from the equator. At 15°, the amplitude of solar radiation reaches about 40 W m^{-2}, which in a local heat balance limit is able to produce a 1° SST variation in a mixed layer of a depth of 50 m. Moreover, the strong coastal upwelling along the eastern boundary in response to variable meridional winds can excite even larger SST variability there (Philander and Pacanowski 1981).

Therefore, in contrast to the ENSO, which is predominantly a free mode in the equatorial ocean–atmosphere system, the annual variability on the equator may consist of a forced response to a large extent. Since the annual solar radiation is weak locally on the equator, the annual forcing effect, if important, can only produce a remote response to the equatorial ocean–atmosphere. That is, the annual variability is first forced by the annual forcing in the extratropics and then somehow propagates to the equatorial region. The remaining fundamental question is then, how does the annual variability in the extratropical ocean–atmosphere system propagates to the equatorial region? This is the fundamental issue to be discussed in the paper.

The amplitude and phase patterns in Figs. 1a,b seem to suggest that a substantial part of annual variability in the eastern equatorial Pacific is produced by the northwestward propagation of variability structure from south of the equator. If propagation is possible for

* Current affiliation: Joint Institute for the Study of the Atmosphere and Oceans, University of Washington, Seattle, Washington.

Corresponding author address: Dr. Zhengyu Liu, Dept. of Atmospheric and Oceanic Sciences, University of Wisconsin–Madison, Madison, WI 53706-1695.

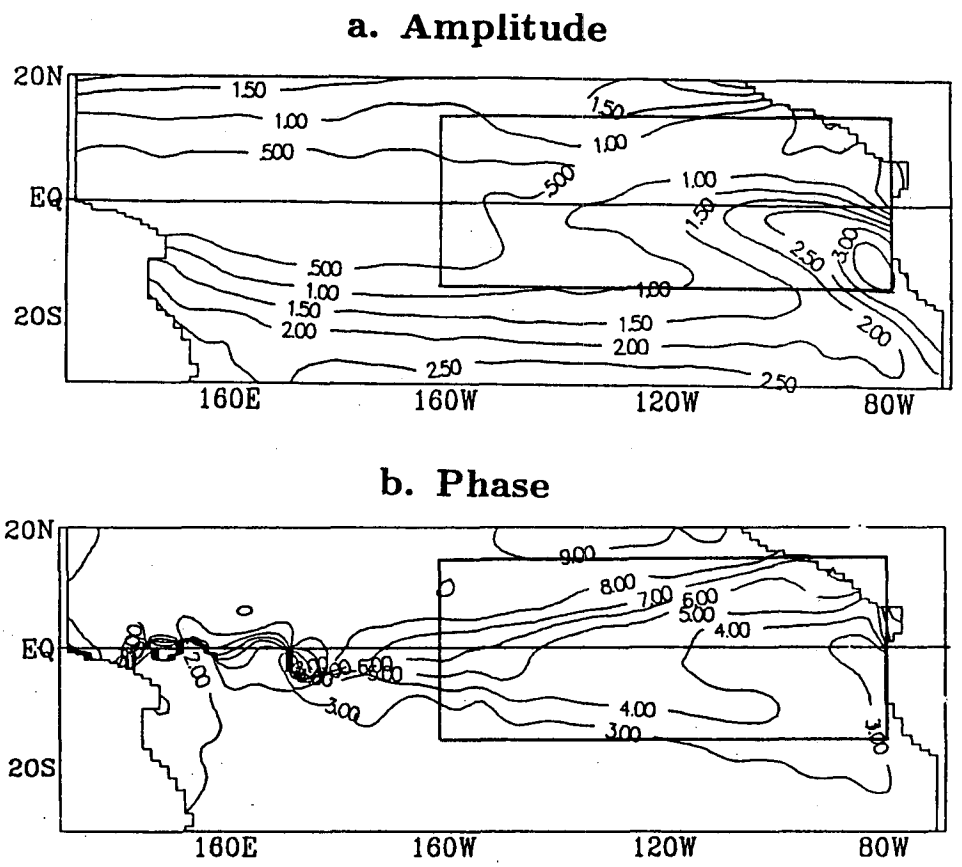

FIG. 1. The (a) amplitude (CI: 0.5°) and (b) phase (CI: 1 mo) of the annual harmonic component SST in the tropical Pacific analyzed from COADS data.

annual variability, it should involve coupling between the ocean and the atmosphere. The atmospheric waves would be too fast. Conversely, the oceanic processes would be too slow. Oceanic Rossby waves can propagate westward and equatorward (e.g., Schopf et al. 1981; Chang and Philander 1989; Liu 1993). The surface mean ocean currents, caused by a mean westward wind and northward wind, can also advect the annual disturbance northwestward, first along the coast and then along the equator. Yet, both are on the order of 10 cm s^{-1} in the zonal direction and even smaller in the meridional direction. At this speed, it will take more than one year for disturbances to reach the central equatorial Pacific from the South American coast.

In this paper, the annual variability in the Tropics is studied with a simple model that couples an atmospheric boundary layer (Lindzen and Nigam 1987) and an oceanic mixed layer. The annual variability is prescribed along the eastern boundary as well as on the extratropical sides of the model domain, where the annual variability is assumed to be produced dominantly by local processes. A spatially varying annual heating, which vanishes on the equator, is also imposed in the SST equation. It is found that the coupling produces a coupled wave, which propagates northward and westward at a reasonable speed. As a result, a significant part of the annual variability in the Tropics is reproduced in the simple model. The coupled wave is a type of SST mode (Neelin 1991). The equatorward and westward propagation is predominantly produced by the coupling due to evaporation and wind mixing entrainment.

This paper is arranged as follows. Section 2 introduces the model. The coupling equation and the propagation of waves will be discussed in section 3. Section 4 discusses the annual variability of SST and winds in the coupled model. Further discussions are presented in section 5.

2. The model

a. *The atmospheric model*

In the tropical eastern Pacific where the SST gradient is large, Lindzen and Nigam (1987) showed that the lower-level atmosphere stationary eddy flows, to a large extent, are forced *locally* by the pressure gradient associated with the SST. This is supported by other

observation and model studies (Gutzler and Wood 1990; Wallace et al. 1989; Wang and Li 1993). Thus, following Lindzen and Nigam, we use the simplest one-layer trade wind boundary layer model

$$-fV = \mu T_x - AU \tag{2.1a}$$

$$fU = \mu T_y - AV, \tag{2.1b}$$

where f is the Coriolis parameter, (U, V) are the anomalous wind velocities, T is the SST, and μ is the thermal forcing parameter. In addition, $1/A = 0.5$ day is the atmospheric dissipation time, corresponding to a dissipation radius of about 8°, represented by the Coriolis parameter value

$$f_A = A. \tag{2.2}$$

A typical thermal forcing parameter in Lindzen and Nigam (1987) is $\mu = 40\ \text{m}^2/(\text{K s}^2)$. On the equator, the A and μ give a 2 m s^{-1} surface wind corresponding to a SST gradient of 1°C/1000 km. (In the following, unless specified, typical values of the parameters used in the paper are listed in Table 1.)

It is important to point out that the model in (2.1) is the simplest version of the Lindzen–Nigam model—the one without "back pressure." In other words, the horizontal pressure gradient at the top of the boundary layer is neglected. A model with interactive back pressure will also include the nonlocal effect of atmospheric dynamics and therefore mask the physics of the propagation due to the air–sea coupling. Nevertheless, the error introduced by the lack of back pressure is limited mainly in the vicinity of the equator. Since we are particularly interested in the equatorward propagation from the extratropics, the error seems unlikely to affect our main results significantly except on the equator. As a first step, we will take the model without back pressure. However, one should keep in mind that the model may produce results rather unrealistic within several degrees of the equator.

b. The ocean model

A simple mixed layer model will be adopted here, with a depth independent of time. The fixed bottom excludes the effect of subsurface thermocline dynamics on the SST but still includes the entrainment, which is part of the upwelling effect. The ocean current is purely wind driven. The pressure-driven currents, which are important in the thermocline, are filtered out. The absence of the thermocline dynamics highlights the surface process and the clear physics of the coupling propagation. Furthermore, although observations suggest that the subsurface dynamics is crucial for the climatologically mean and interannual variation of SST, recent observations seem to suggest that the subsurface dynamics is not crucial for the annual cycle in the eastern equatorial Pacific. Indeed, the thermocline depth changes dramatically at the interannual timescale, but it changes little at the annual timescale [e.g., Fig. 8a of McPhaden and Taft (1988)]. Thus, the assumption of a fixed depth of mixed-layer bottom seems to be a reasonable starting point for the study of the annual variability.

TABLE 1. Standard parameters used in the calculation.

Parameter	Meaning	Value
A	1/atmospheric damping time	2×10^{-5} s^{-1}
μ	thermal forcing coefficient	0.4×10^2 m^2/(K s^2)
c_p	heat content	4.18×10^3 J(kg)$^{-1}$ K^{-1}
c_E	Dalton number	1.5×10^{-3}
L_v	latent heat of vaporization	2.5×10^6 J (kg)$^{-1}$
ρ_a	density of air	1.2 kg m^{-3}
ρ_0	density of water	1.0×10^3 kg m^{-3}
m	wind mixing coefficient	1.5
g	gravity acceleration	10 m s^{-2}
c_D	drag coefficient	1.5×10^{-3}
α	thermal expansion coefficient	3×10^{-4} K^{-1}
K_T	1/SST damping time	1.7×10^{-7} s^{-1}
γ	wind forcing coefficient	2.3×10^{-7} s^{-1}
K_m	1/surface current damping time	2×10^{-6} s^{-1}

The mixed layer model is essentially the Kraus–Turner model (Kraus and Turner 1967), which is written for total SST as

$$(\partial_t + u\partial_x + v\partial_y + K_T^*)T = \left[\frac{Q_t}{\rho_0 c_p} - w_e \Delta T\right] \Big/ h. \tag{2.3a}$$

Here the total external heat flux Q_t can be decomposed into shortwave heating Q_{short}, longwave cooling Q_{long}, and evaporation cooling $Q_E = L_v \rho_a c_E \Delta q |\mathbf{V}_a|$ as $Q_t = Q_{\text{short}} - Q_{\text{long}} - Q_E$, where Δq equals $q_s - q_a$ with $q_s(T)$ as the surface specific humidity (assuming saturated) and q_a as the specific humidity at a standard level, and $\mathbf{V}_a$ is the total wind velocity at a standard level. Other parameters are defined as in Table 1. The entrainment of temperature from below is derived from the turbulent energy balance as

$$w_e \Delta T = \frac{2mu_*^3}{\alpha g h} - \frac{Q_t}{\rho_0 c_p}, \tag{2.3b}$$

where w_e and ΔT are, respectively, the entrainment velocity and the temperature jump across the bottom of the mixed layer, h is the depth of the mixed layer, m is the wind mixing coefficient, $u_* = \sqrt{\tau/\rho_0}$ is the frictional velocity, $\tau = \rho_a c_D (|\mathbf{V}_a|)^2$ is the wind stress, and other parameters are listed in Table 1. One may refer to Anderson and McCreary (1985) and Xie et al. (1989) for a more detailed derivation of (2.3).

Separating the variables into mean and perturbation parts,

$$T = \bar{T} + T', \quad (u, v) = (\bar{u}, \bar{v}) + (u', v'),$$

$$(U_a, V_a) = (\bar{U}, \bar{V}) + (U', V'),$$

one obtains the perturbation SST equation as (primes have been dropped)

$$(\partial_t + K_T + \bar{u}\partial_x + \bar{v}\partial_y)T + u\bar{T}_x + v\bar{T}_y = \frac{2}{\rho_0 c_p h}\left[Q_R - \left(1 + \frac{3h_E}{2h}\right)\bar{Q}_E \frac{\bar{U}U + \bar{V}V}{\bar{U}^2 + \bar{V}^2}\right], \quad (2.4a)$$

where Q_R is the anomalous shortwave radiation heating, $\bar{Q}_E$ is the mean evaporation cooling, $h = 50$ m is the mixed layer depth, and h_E is a pseudo Monin–Obukov ocean depth due to evaporation:

$$h_E = \frac{2m\bar{u}_*^3}{\alpha g} \Big/ \frac{\bar{Q}_E}{\rho_0 c_p}. \quad (2.4b)$$

The coefficient $1/K_T = 70$ days is the local damping time for an SST anomaly, which includes the effect due to the temperature dependence of latent heat flux, eddy mixing, and longwave radiation (Xie et al. 1989). The wind anomaly comes from two effects: the wind mixing entrainment and evaporation. The ratio between the two effects are

$$\frac{\text{entrainment}}{\text{evaporation}} = \frac{3h_E}{2h}.$$

With a typical mean evaporation cooling rate $\bar{Q}_E = 60$ W m^{-2}, we have $h_E = 29$ m. Therefore, the effect of evaporation and wind mixing entrainment is comparable. It should be pointed out that in this linearized form the background gustiness is not considered.

The last term in (2.4a) is due to the effect of variation of total wind speed on evaporation and entrainment. For example, an anomalous westward wind ($U < 0$), in the presence of a mean westward trade wind ($\bar{U} < 0$), increases the magnitude of the total westward wind. The increased wind cools the SST ($T_t \sim -\bar{U}U < 0$) through both the increased evaporation and intensified wind mixing of the mixed layer.

Finally, in the surface mixed layer, the momentum equations for anomalous ocean currents are taken to be simply in the wind-driven balance:

$$-fv = \gamma U - K_m u \quad (2.5a)$$

$$fu = \gamma V - K_m v. \quad (2.5b)$$

The momentum damping $1/K_m$ is about 6 days. This corresponds to an oceanic disspation radius of about 1° where

$$f_O = K_M. \quad (2.6)$$

The wind forcing coefficient $1/\gamma$ is about 50 days. Thus, a wind disturbance of 1 m s^{-1} produces a current 10 cm s^{-1} on the equator. Similar parameters have been used in previous works (e.g., Philander et al. 1984; Yamagata 1985; Hirst 1986). As discussed before, to highlight the effect of the dynamics within the mixed layer, pressure gradient within and at the bottom of the oceanic mixed layer is neglected.

3. The coupling and wave rays

a. The coupling equation

Using (2.1), the wind can be represented in terms of SST gradient as

$$U = \frac{\mu}{f^2 + A^2}(fT_y + AT_x) \quad (3.1a)$$

$$V = \frac{\mu}{f^2 + A^2}(-fT_x + AT_y). \quad (3.1b)$$

With (2.5), the anomalous ocean currents can be represented in terms of wind as

$$u = \frac{\gamma}{f^2 + K_m^2}(fV + K_m U) \quad (3.2a)$$

$$v = \frac{\gamma}{f^2 + K_m^2}(-fU + K_m V). \quad (3.2b)$$

Since the wind is related to SST gradient as in (3.1), the current in (3.2), which is caused by air–sea coupling, is also related to SST gradient. Consequently, in the SST equation (2.4a), both the advection of mean SST gradient and the evaporation–entrainment can be represented in terms of T_x and T_y. This gives a single prediction equation for SST as

$$(\partial_t + K_T)T + (\bar{u} + C_x)\partial_x T + (\bar{v} + C_y)\partial_y T = \frac{2}{\rho_0 c_p h} Q_R, \quad (3.3)$$

where (C_x, C_y) is the propagation speed of the coupled waves, which will be discussed in detail soon. This equation is a forced first-order linear partial differential equation; its left-hand side represents nondispersive two-dimensional waves propagating at the total wave speed or characteristic speed:

$$\frac{dt}{ds} = 1 \quad (3.4a)$$

$$\frac{dx}{ds} = \bar{u} + C_x \quad (3.4b)$$

$$\frac{dy}{ds} = \bar{v} + C_y. \quad (3.4c)$$

The SST evolves along a characteristic according to

$$\frac{dT}{ds} = \frac{2}{\rho_0 c_p h} Q_R - K_T T. \quad (3.4d)$$

Now, the subsurface dynamics is ignored.

In the above, (C_x, C_y) is the wave speed due to air–sea coupling. It has two parts: the evaporation–entrainment part C_E and the SST gradient part C_T; that is,

$$(C_x, C_y) = (C_{Ex} + C_{Tx}, C_{Ey} + C_{Ty}) \quad (3.5a)$$

$$(C_{Ex}, C_{Ey}) = m_1(u_E - F_1 v_E, v_E + F_1 u_E) \quad (3.5b)$$

$$(C_{Tx}, C_{Ty}) = m_1 m_2(m_3 u_T - F_2 v_T, m_3 v_T + F_2 u_T). \quad (3.5c)$$

Here m_1, m_2, m_3, F_1, and F_2 are latitude-dependent, nondimensional coupling coefficients:

$$m_1(f) = 1 \Big/ \left[1 + \left(\frac{f}{f_A}\right)^2\right] > 0 \quad (3.6a)$$

$$m_2(f) = 1 \Big/ \left[1 + \left(\frac{f}{f_O}\right)^2\right] > 0 \quad (3.6b)$$

$$m_3(f) = 1 - \frac{f^2}{f_A f_O} \quad (3.6c)$$

$$F_1(f) = \frac{f}{f_A} \quad (3.6d)$$

$$F_2(f) = \frac{f}{f_O}\left(1 + \frac{f_O}{f_A}\right), \quad (3.6e)$$

where f_A and f_O are dissipation radius of the atmosphere and the mixed layer [see (2.2) and (2.6)].

In the evaporation–entrainment part C_E, we have defined

$$(u_E, v_E) = \frac{\mu}{A} E_e(\bar{U}, \bar{V}), \quad (3.7)$$

where

$$E_e = \frac{2\left(1 + \dfrac{3h_E}{2h}\right)}{\rho_0 c_p h} \frac{\bar{Q}_E}{(\bar{U}^2 + \bar{V}^2)}.$$

Equation (3.7) states that a stronger mean evaporation $\bar{Q}_E$ or a shallower mixed layer depth h produces a faster propagation speed.

The other part of propagation C_T comes from the advection by the current anomaly of the mean SST field. In this part,

$$(u_T, v_T) = \frac{\mu\gamma}{AK_m}(\bar{T}_x, \bar{T}_y). \quad (3.8)$$

A stronger mean SST gradient produces a faster propagation speed.

It is also interesting to notice that, away from the equator (that is, for very large f such that $f/f_A, f/f_O \to \infty$), the coupling propagation speed (C_x, C_y) vanishes [see (3.5) and (3.6)]. Therefore, (3.3) shows that SST is decoupled from the atmosphere and is advected simply by the mean ocean current. This occurs because at higher latitude, the temperature gradient tends to force a weaker wind, as shown in (3.1). Thus, the coupling is reduced. Furthermore, if the mean current is weak, the SST equation (3.3) simplifies to the local heat budget $(\partial_t + K_T)T = 2Q_R/\rho_0 c_p h$.

b. The wave ray

Before exploring details of the wave rays, we first compare the relative contributions of C_E and C_T to the coupling wave speed. In the vicinity of the equator $(f \to 0)$, (3.5) and (3.6) yield $(C_{Ex}, C_{Ey}) = (u_E, v_E)$ and $(C_{Tx}, C_{Ty}) = (u_T, v_T)$. Furthermore, with a typical mean wind speed $\sqrt{\bar{U}^2 + \bar{V}^2} = 5$ m s^{-1} and a mean SST gradient $|\nabla\bar{T}| = 1°\text{C}/1000$ km, one can estimate $|\mathbf{v}_E| \approx 0.5$ m s^{-1} and $|\mathbf{v}_T| \approx 0.25$ m s^{-1}. Thus, the contribution to the wave speed from the evaporation–entrainment and mean SST gradient are comparable; that is,

$$\frac{C_E}{C_T} \sim 1 \quad \text{as} \quad f \to 0. \quad (3.9a)$$

Far away from the equator where $f/f_A, f/f_O \to \infty$, Eq. (3.2) shows that the current decreases faster than the wind. Since C_E involves only the wind while C_T involves the current, one should expect a dominant C_E. Indeed, from (3.5) and (3.6), one obtains

$$\frac{C_E}{C_T} \sim O\left(\frac{f}{f_O}\right) \gg 1, \quad \text{as} \frac{f}{f_O} \to \infty. \quad (3.9b)$$

Equations (3.9a,b) suggest that the evaporation–entrainment effect is dominant except in the vicinity of the equator. In the following, we study the propagation of coupled waves in more detail.

1) MEAN ZONAL WIND INFLUENCE

In the presence of a mean zonal wind alone, the wave speed in (3.5) becomes

$$(C_x, C_y) = m_1 u_E(1, F_1). \quad (3.10)$$

In the Tropics, a mean westward wind $\bar{U} < 0$ prevails, which corresponds to a $u_E < 0$ in (3.7). The resulting propagation is westward $(C_x < 0)$ and equatorward $(C_y \sim -f)$. Physically, to the west of an initial warm anomaly, there is an eastward anomalous SST gradient T_x (see the schematic Fig. 2a). This SST gradient produces an eastward (westward) wind and therefore reduces the mean westward wind there. Thus, the evaporation and wind mixing entrainment is reduced there, the SST is warmed, and the warm anomaly then propagates westward. This westward propagation for annual (and interannual) disturbances seems to be consistent with observations (Horel 1982) and some coupled GCM experiments (Meehl 1990; Lau et al. 1992).

The equatorward meridional propagation under a mean eastward wind is explained schematically in Fig.

2b. In the Northern Hemisphere, to the south of an initial warm anomaly, a northward anomalous temperature gradient exists. Geostrophy then requires an eastward wind there, which reduces the total westward wind and in turn evaporation and entrainment. The warm anomaly then propagates southward.

One example of the wave ray in (3.11) is presented in Fig. 3a. The basic state is a westward wind of intensity 3 m s^{-1}. Three groups of characteristics (wave rays) are plotted. The first group starts from the eastern boundary, and the other two groups start from the northern and southern boundaries at the latitudes of ±15°, respectively. The rapid westward and equatorward propagation is obvious. In two months, the coupled wave has propagated 20° westward and 10° equatorward.

2) MEAN MERIDIONAL WIND INFLUENCE

In the presence of a mean meridional wind alone, (3.5) gives the wave speed

$$(C_x, C_y) = m_1 v_E(-F_1, 1). \qquad (3.11)$$

In the Tropics, there is typically a symmetric mean wind component converging toward the equator $\bar{V} \sim -f$. With (3.6) and (3.11), this $\bar{V}$ produces an eastward ($C_x > 0$) and equatorward ($C_y \sim -f$) propagation. The physical mechanism can be explained similarly to those in Figs. 2a,b. This zonal propagation is opposite to that caused by the mean westward wind, but the equatorward convergence of wave rays reinforces the propagation due to the mean westward wind. One example with a mean meridional wind $\bar{V} = -2\phi/10$ m s^{-1} (ϕ is the latitude in degrees) is presented in Fig. 3b. Both the zonal and meridional propagation speeds are comparable to those in Fig. 3a, which occurs in the presence of a mean westward wind.

In the eastern tropical Pacific, there is also a strong mean northward wind component $\bar{V} > 0$ across the equator. According to (3.11) and (3.6), this mean northward wind will produce a northward propagation in the meridional direction ($C_y > 0$) in both hemispheres, a westward propagation in the Northern Hemisphere and an eastward propagation in the Southern Hemisphere ($C_x \sim -f$). One example with a uniform $\bar{V} = 2$ m s^{-1} is shown in Fig. 3c. The northward wind will push the wave rays across the equator to converge in the Northern Hemisphere. It decelerates the westward propagation to the south of the equator but accelerates the westward propagation to the north of the equator.

3) MEAN ZONAL SST GRADIENT INFLUENCE

In the presence of a mean zonal SST gradient $\bar{T}_x < 0$, as in the tropical ocean, (3.8) yields $u_T < 0$. Thus, (3.5) gives the phase speed

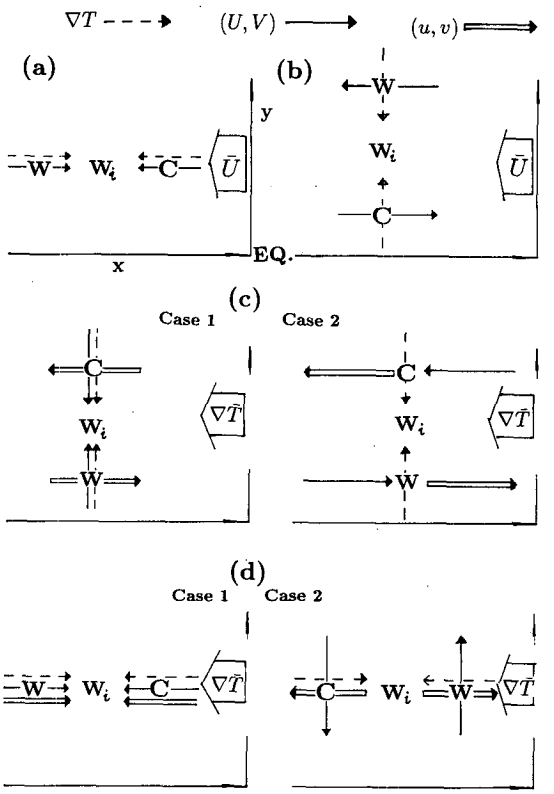

FIG. 2. Schematic figure of the physical mechanisms for the propagation of coupled boundary layer waves in the Northern Hemisphere. (a) Zonal propagation (westward) due a mean westward wind. (b) Meridional propagation (southward) due to a mean westward wind. (c) Meridional propagation due to a mean westward temperature gradient. The propagation is southward for both cases. (d) Zonal propagation due to a mean westward temperature gradient; the propagation is westward in case 1 but eastward in case 2. In all panels, warm and cold SST anomalies are represented by W and C, with the initial warm anomaly subscripted *i*. The mean easterly wind $\bar{U} < 0$ and the westward mean SST gradient $\nabla\bar{T} < 0$ are also shown schematically on the right of each panel.

$$(C_x, C_y) = m_1 m_2 u_T(m_3, F_2). \qquad (3.12)$$

The meridional speed is equatorward ($C_y \sim -f$). Physically, to the south of an initial warm SST anomaly, there exists a northward SST gradient. Then, there are two mechanisms both favoring an equatorward propagation, as explained schematically in Fig. 3c. In the first case, a directly driven northward wind is forced to the south of the warm anomaly, which drives a westward Ekman drift. Since the mean SST decreases toward the east, this eastward current tends to warm the SST there. The warm anomaly, then, moves southward. In the second case, to the south of the anomaly, geostrophy requires an eastward wind, which directly drives an eastward current and a warm advection. Then, like the first case, the warm anomaly moves southward.

Since the coupling coefficient m_3 changes sign at the coupled dissipation radius [see (3.6c)],

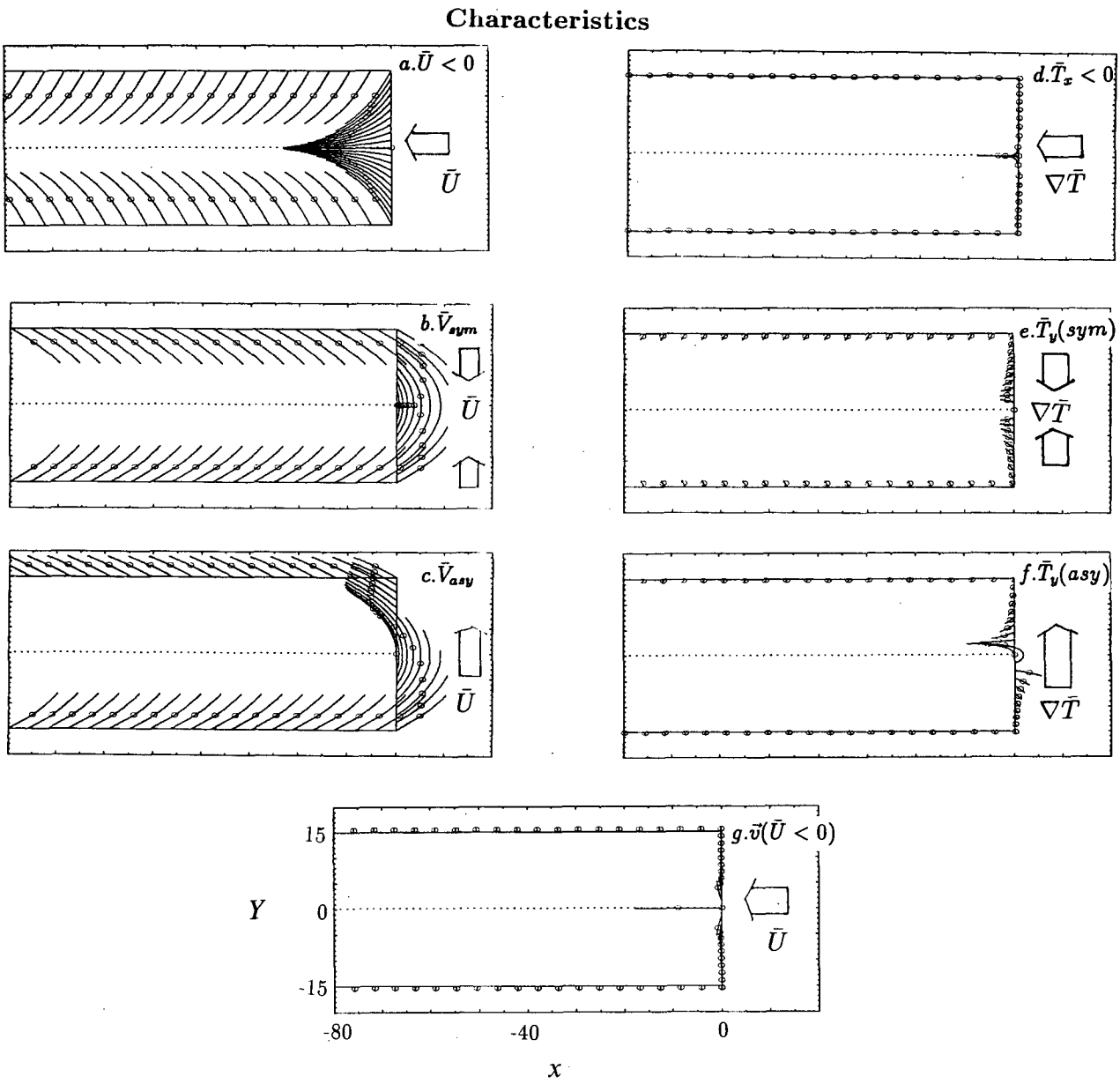

FIG. 3. The characteristics due to some simple basic states. On each characteristic curve, a circle marks the distance traveled after one month. The different mean states are (a) westward wind $\bar{U} = -3$ m s^{-1}, (b) symmetric meridional wind case with $\bar{V} = -2\phi/10$ m s^{-1} (ϕ is latitude in degrees), (c) asymmetric meridional wind case with $\bar{V} = 2$ m s^{-1}, (d) zonal SST gradient case with $\bar{T} = -5$°C $\lambda/80$ (λ in degrees of longitude), (e) symmetric meridional SST gradient case with $\bar{T} = -6$°C $\times$ $(\phi/20)^2$, (f) asymmetric SST gradient case with $\bar{T} = 4$°C $\phi/20$, (h) mean ocean current forced by a mean wind of $\bar{U} = -3$ m s^{-1} using Eq. (2.4). The directions of the mean wind and mean SST gradient are also shown schematically on the right side in each panel.

$$f_M = \sqrt{AK_m} = \sqrt{f_A f_O} \qquad (3.13)$$

(about 3° for the value in Table 1), the zonal speed changes sign too. The propagation is westward within $\pm f_M$, but eastward beyond $\pm f_M$. The physics is explained in Fig. 3d. An initial warm anomaly produces an anomalous eastward SST gradient on its west. This SST gradient then enables two mechanisms to function, which move the anomaly in the opposite directions. In the first case, a down-pressure-gradient eastward wind is produced to the west of the anomaly, which in turn drives an eastward current or a warm advection of the mean SST. Thus, the warm SST anomaly propagates westward. In the second case, geostrophy requires a northward wind to the east of the warm anomaly, which in turn drives a westward Ekman drift and a cold advection. Thus, the warm anomaly moves eastward. Obviously, the first mechanism is dominant near the equa-

tor because it depends on the directly driven wind and current. The second mechanism prevails away from the equator where geostrophy and Ekman drift dominate. The critical latitude is the mixed dissipation radius in (3.13).

With a typical mean $\bar{T}(x) = -5°C\lambda/80$ (λ in degrees of longitude), the wave rays are shown in Fig. 3d. The most striking difference from Figs. 3a–c is that the propagation speed is very slow except in the vicinity of the equator. This agrees with the scaling analysis in (3.9).

4) MEAN MERIDIONAL SST GRADIENT INFLUENCE

With a mean meridional SST gradient alone, (3.5) gives the phase speed

$$(C_x, C_y) = m_1 m_2 v_T(-F_2, m_3). \qquad (3.14)$$

As an example, a cold tongue in the mean SST ($\bar{T}_y \sim f$) gives westward propagation in the zonal direction ($C_x < 0$). The meridional propagation is northward beyond $\pm f_M$ but southward within $\pm f_M$. The physical mechanism can be understood similar to the mean zonal gradient case as in Figs. 3c,d. In the eastern Pacific, the mean cold tongue builds a mean northward SST gradient $\bar{T}_y > 0$. One can check that this gives a westward propagation in the Northern Hemisphere but an eastward propagation in the Southern Hemisphere. The meridional propagation is northward within $\pm f_M$ but southward beyond $\pm f_M$.

Figures 3e and 3f present two examples with, respectively, a symmetric mean $\bar{T} = -6°C \times (\phi/20)^2$ and an asymmetric $\bar{T} = 4°C\ \phi/20$ (ϕ in degrees of latitude). In general, the wave speed increases toward the equator (for the symmetric case, on the equator, $\bar{T}_y = 0$ and the wave speed is zero). As shown in (3.9), except near the equator, the wave speed is negligible compared with that caused by evaporation–entrainment.

5) MEAN CURRENT INFLUENCE

The determination of the mean current is beyond the scope of this paper. Here, we simply apply Eq. (2.5) to the mean current too. This is not legitimated. However, it seems likely that the magnitude of mean currents will not be changed significantly, and therefore the errors introduced will not be serious. In any case, it seems reasonable to have a mean current advection comparable to the anomalous advection on the mean SST gradient; that is, $\bar{u}\bar{T}_x \sim u\bar{T}_x$. Thus, from (3.9), we should also expect that the mean current is insignificant except near the equator. With (2.5) for the mean current forced by a mean zonal wind of -3 m s^{-1} as in Fig. 3a, the characteristics are drawn in Fig. 3g. One sees that a strong westward mean current exists in the equator. Elsewhere, the divergent Ekman drift and westward propagation are negligible compared with those in Fig. 3a. Similar results can be found for the mean current forced by the mean meridional wind.

In short, in both the meridional and zonal directions, the evaporation–entrainment mechanism is able to produce a rapid propagation of coupled disturbance over the whole Tropics. Near the equator, the propagation is more complex. Mean SST gradients and mean currents may also induce significant wave propagation. But, several degrees away from the equator the effect of mean SST gradients and mean currents are negligible. Therefore, the propagation of extratropical annual signal toward the equator depends mainly on the evaporation–entrainment mechanism.

In Fig. 4c, we present a composite wave ray. The mean wind and SST fields are shown in Figs. 4a,b, which are approximately the sum of the wind and SST

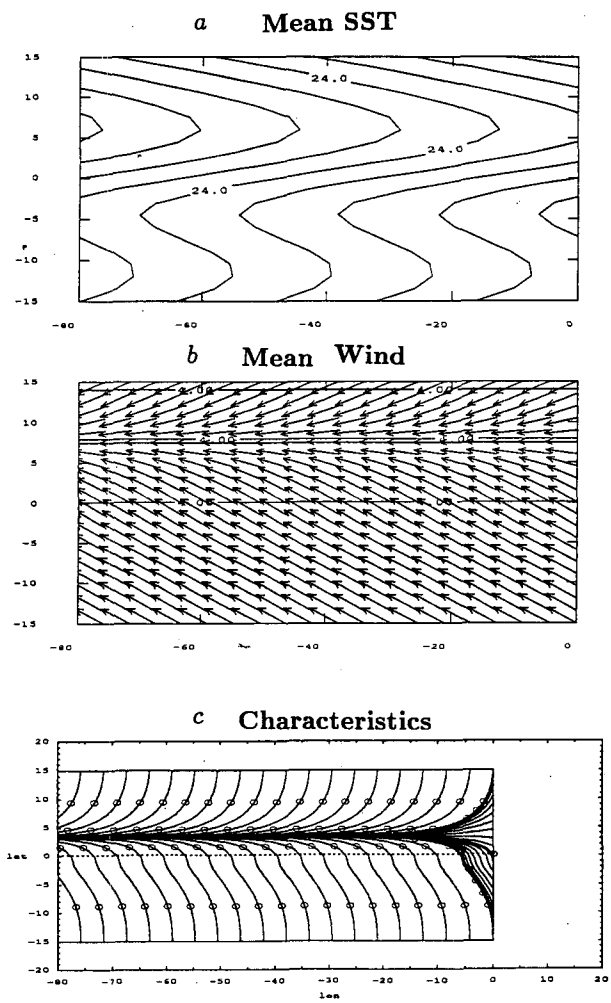

FIG. 4. The mean SST field (a), mean wind field (b), and the resulting total characteristics field (including mean ocean current) (c). An asymmetric meridional wind and a meridional SST gradient have been added in the mean field (a) and (b). The total wind speed is also contoured in (b) (CI: 1 m s^{-1}). The mixed layer depth is 50 m, uniform everywhere for the characteristics in (c).

fields in Figs. 3a–g, and which include some basic features of the eastern tropical Pacific. For simplicity, no zonal variation in the $\bar{U}$, $\bar{V}$, $\bar{T}_x$, $\bar{T}_y$ fields is imposed. Several features are noteworthy. First of all, the wave rays propagate rapidly equatorward and westward across the domain (80° × 30°) in three months. This speed is consistent with that from observations (Fig. 1b). Second, the overall pattern of wave rays is similar to that determined by the evaporation–entrainment mechanism alone (see Figs. 3a–c), except near the equator. Finally, the asymmetric part of the mean states $\bar{V}$ and $\bar{T}_y$ makes the waves penetrate across the equator, converging on a latitude in the Northern Hemisphere.

4. Evolution of coupled annual variability

With the prediction equation (3.3) in its characteristic form (3.4), we will solve the equation along the characteristics. First, we discuss the external heating and the boundary conditions for the characteristics.

a. The forcing and solution

The radiation forcing takes the form

$$Q_R(y, t) = Q(y) \cos[\omega t - \theta_Q(y)], \quad (4.1)$$

where $Q(y)$ and θ_Q are, respectively, the amplitude and phase of the heating, and ω is the frequency. As shown in Fig. 5a (R. C. Pacanowski 1992, personal communication), $Q(y)$ increases linearly from zero on the equator to about 40 W m^{-2} at 15°. Using pure local heat balance, this heating would produce an anomalous SST with the amplitude of about 1°C at 15° in a mixed layer of 50 m. The phase drawn in Fig. 5a states that the Southern and Northern Hemisphere receive the maximum heating in January and July, respectively.

The anomalous SST along the eastern, southern, and northern boundaries are to simulate the gross features in the observation (Fig. 1). The eastern boundary SST is

$$T(x = 0, y, t) = T_e(y) \cos[\omega t - \theta_{Te}(y)]. \quad (4.2)$$

The amplitude $T_e(y)$ and phase θ_{Te} for calculation are shown in Fig. 5b. The maximum SST is achieved along the eastern boundary in March. The SST along the southern and northern boundaries are, respectively,

$$T(x, y = 15°, t) = T_s(x) \cos[\omega t - \theta_{Ts}(x)] \quad (4.3)$$

and

$$T(x, y = -15°, t) = T_n(x) \cos[\omega t - \theta_{Tn}(x)]. \quad (4.4)$$

The amplitudes and phases are plotted in Fig. 5c. The southern boundary SST reaches its maximum along −15° in March, while the Northern Hemisphere SST achieves its maximum along 15° in September. In reality, this southern boundary SST anomaly should be closely related to the subtropical high over the southern Pacific, as observed by van Loon and Shea (1985). A detailed study of the extratropical ocean–atmosphere system is beyond the scope of the present paper.

Since the computation domain is covered by characteristics initiating from the eastern, southern, and northern boundaries as seen in Fig. 4c, the SST throughout the domain can be obtained by solving the characteristic equations (3.4). Along one characteristic $x = x^*(s)$, $y = y^*(s)$ derived from (3.4b,c); the solution of SST can be derived from (3.4d) as

$$T(x, y, t) = \mathrm{Re}\left\{ e^{i\omega t}\left[T_i e^{-(i\omega + K_T)s} + \frac{2}{\rho_0 c_p} \int_0^s \frac{e^{(i\omega + K_T)(s^* - s)}}{h} Q[y^*(s^*)] ds^* \right] \right\}.$$

One can then obtain the SST solution in the form of

$$T = T(x, y) \cos[\omega t - \theta(x, y)]. \quad (4.5a)$$

Here $T(x, y)$ and $\theta(x, y)$ are the amplitude and phase of the annual variability.

b. Evolution of the coupled annual disturbances

With the characteristic field in Fig. 4c, the amplitude and phase of the SST solution (4.5) are plotted in Fig. 6. With the eastern boundary forcing (4.2) alone, the amplitude and phase are shown in Figs. 6a,b, respectively. From the eastern boundary south of the equator, an amplitude tongue extends northwestward toward the interior. However, the amplitude is limited within about 20 degrees of the eastern boundary. Since the heating is absent, the phase is simply the line of constant characteristic distance from the eastern boundary. (The contour becomes zero beyond the influence zone of the eastern boundary.)

When the southern and northern boundary SST forcings (4.3a,b) are added, the amplitude and phase of SST anomaly are shown in Figs. 6c,d. The SST variability is increased substantially toward the interior due to the equatorward convergence of wave rays. The variability tongue now extends deep into the interior from the southeastern corner. However, the zonal propagation of the tongue remains slow near the equator. The phase is the same as the pattern of characteristics in Fig. 4c. One unrealistic feature is that north of the convergence latitude, the phase decreases toward the north, opposite to the observation (Fig. 1b). This is simply because that region is influenced only by the northern boundary SST, which propagates southward.

With the local heating (4.1) alone [i.e., $T_e(y) = T_s(x) = T_n(x) = 0$], the amplitude and phase of the forced SST variability are presented in Figs. 6e,f. Note that since we have set $T_s = T_n = 0$, the solution in Figs. 6e,f only represents the accumulated effect of the forcing along characteristics. Therefore, although the heating reaches a maximum at 15° and vanishes on the equator, the forced solution has maximum amplitude in the interior.

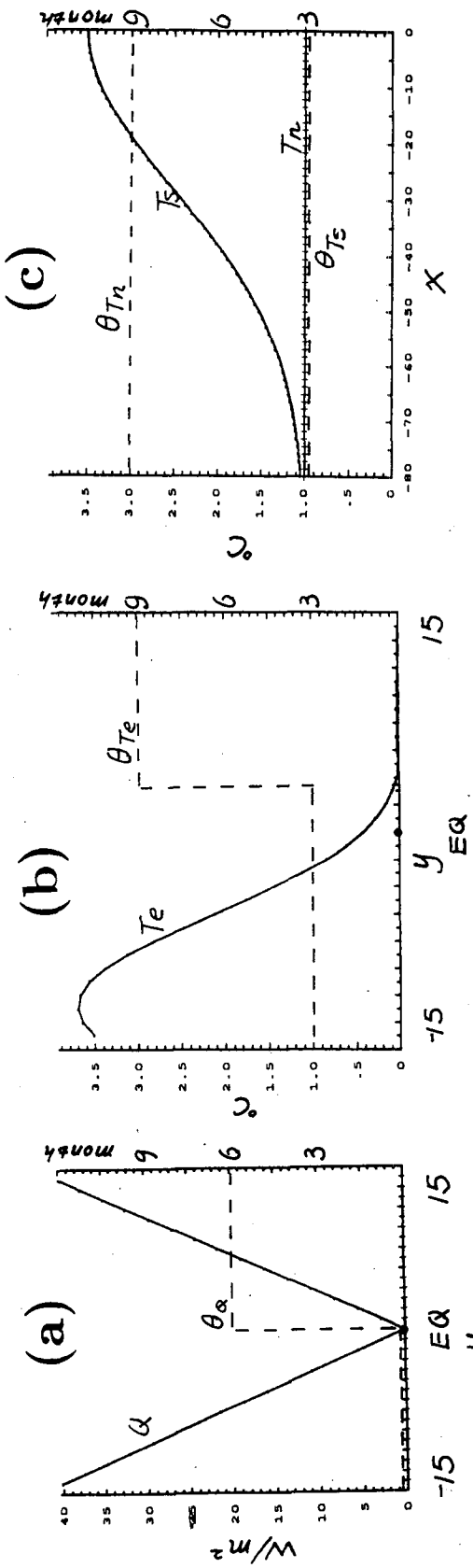

FIG. 5. The amplitude and phase of the forcing and boundary conditions for (a) radiation heating as a function of latitude, (b) the eastern boundary SST as a function of latitude, and (c) the southern and northern SST as a function of longitude. Solid lines are amplitude; dashed lines are phase.

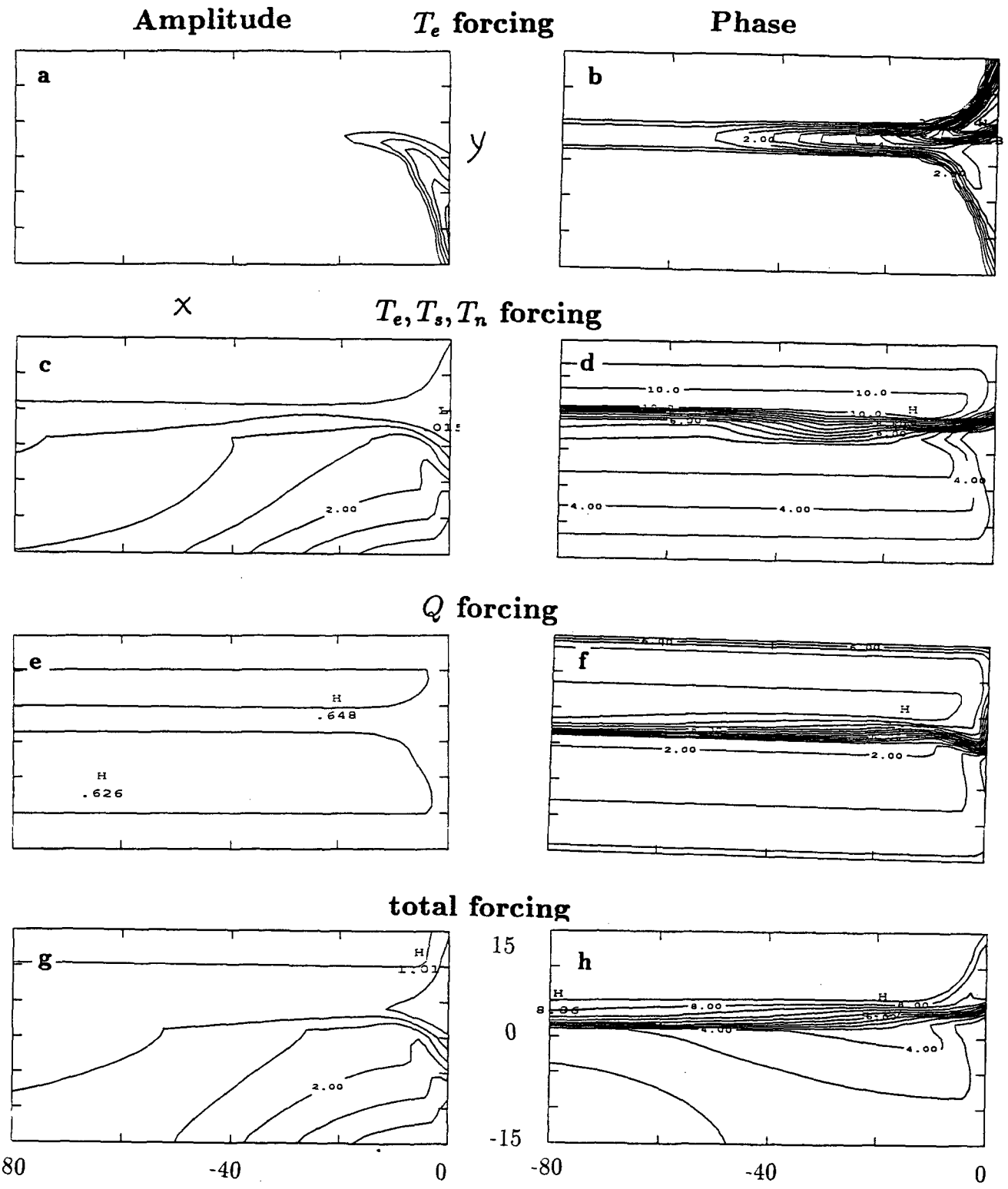

FIG. 6. The amplitude (CI: 0.5°) and phase (CI: 1 mo) of the forced SST solution evolved under the characteristic field of Fig. 4c where (a) and (b) are forced by the eastern boundary SST in Fig. 5b, (c) and (d) are forced by the SST in the eastern, southern, and northern boundaries in Figs. 5b,c, (e) and (f) are forced by the heating in Fig. 5a, and (g) and (h) are due to all the forcings in Figs. 5a–c.

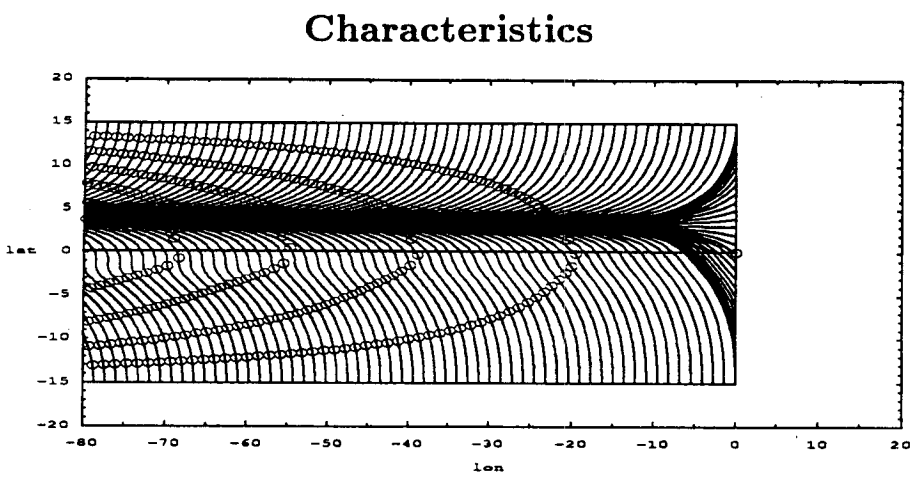

FIG. 7. As in Fig. 4c but with an oceanic mixed layer deepening linearly from 25 m at the eastern boundary to 100 m 80 degrees to the west. Compared with Fig. 4c, the westward propagation is enhanced near the eastern boundary.

It should be pointed out that the converging characteristics would build a meridional SST front in the latitude of convergence, because SST tends to have a small amplitude at the latitude of convergence but a large amplitude away from that latitude. Indeed, the characteristics reaching the latitude of convergence start from the eastern boundary near the equator (see Fig. 4c) where both the heat forcing (Q) and boundary SST (T_e) are small. On the other hand, the converging characteristics increase the amplitude of variability near that latitude by either specifying greater boundary SST or accumulated larger heating. We will return to this point later.

Finally, if the heating is added to the boundary SST forcing, the amplitude and phase of annual SST variability are shown in Figs. 6g,h. The amplitude of the SST remains similar to Fig. 6c, where the heating is absent. The phase is improved north of the convergence latitude. Now, it increases northward. In addition, in the southwest quarter of the domain, where the boundary SST amplitude is small, the phase exhibits an eastward propagation tendency, as in observations (Fig. 1b), but the simulated eastward tendency is too strong.

Overall, although the equatorward propagation is produced reasonably well in Figs. 6g,h, the westward propagation, particularly in the vicinity of the equator, is underestimated. One way to improve the simulation is to improve our crude mean state representation. For example, the mean state in the Tropics varies substantially in the zonal direction, which has been neglected before. One important feature is the sharp eastward shallowing of the mixed layer depth toward the eastern equatorial region. This could influence the wave speed significantly. A shallow mixed layer in the east should enhance the evaporation–entrainment effect and therefore accelerate the wave rays. Thus, one should expect an enhanced westward propagation, particularly near the eastern boundary, due to a westward deepening of the mixed layer. This is indeed the case. We still use the mean wind and SST field in Figs. 4a,b. The mixed layer depth, however, is now $h = h(x)$, which deepens linearly toward the west from 25 m on the eastern boundary to 100 m at −80°. The derived characteristics are shown in Fig. 7. Compared with Fig. 4c, the westward propagation is clearly improved near the eastern boundary, but not substantially, especially near the equator. In the western part of the domain, the propagation is slowed down significantly due to a deeper mixed layer.

The amplitude and phase of the annual SST anomaly under the forcing in Fig. 5 are presented in Fig. 8. Compared with Fig. 6, for a constant mixed layer depth the eastern boundary forced disturbance extends farther west (Fig. 8a). Adding the southern and northern boundary SST forcing (Fig. 8c), the westward propagation in the eastern part is also improved, but not significantly, particularly in the vicinity of the equator. The westward propagation along the equator remains slow. This also shows up in the phase diagram (Fig. 8d), which basically reflects the pattern of characteristics in Fig. 7. Thus, there is still a lack of a salient westward tongue of amplitude along the equator, inconsistent with observations (Figs. 1a,b). A further improvement (compared with Fig. 6c) is that the amplitude (say, the 0.5° contour) now does show a pattern similar to observations, which is separated in the middle basin by the larger amplitude tongue from the southeast. This is caused by the faster westward propagation, which produces a deeper penetration of the tongue.

The heat-induced variability (Figs. 8e, f) are similar to the previous case (Figs. 6e, f) with a slightly altered

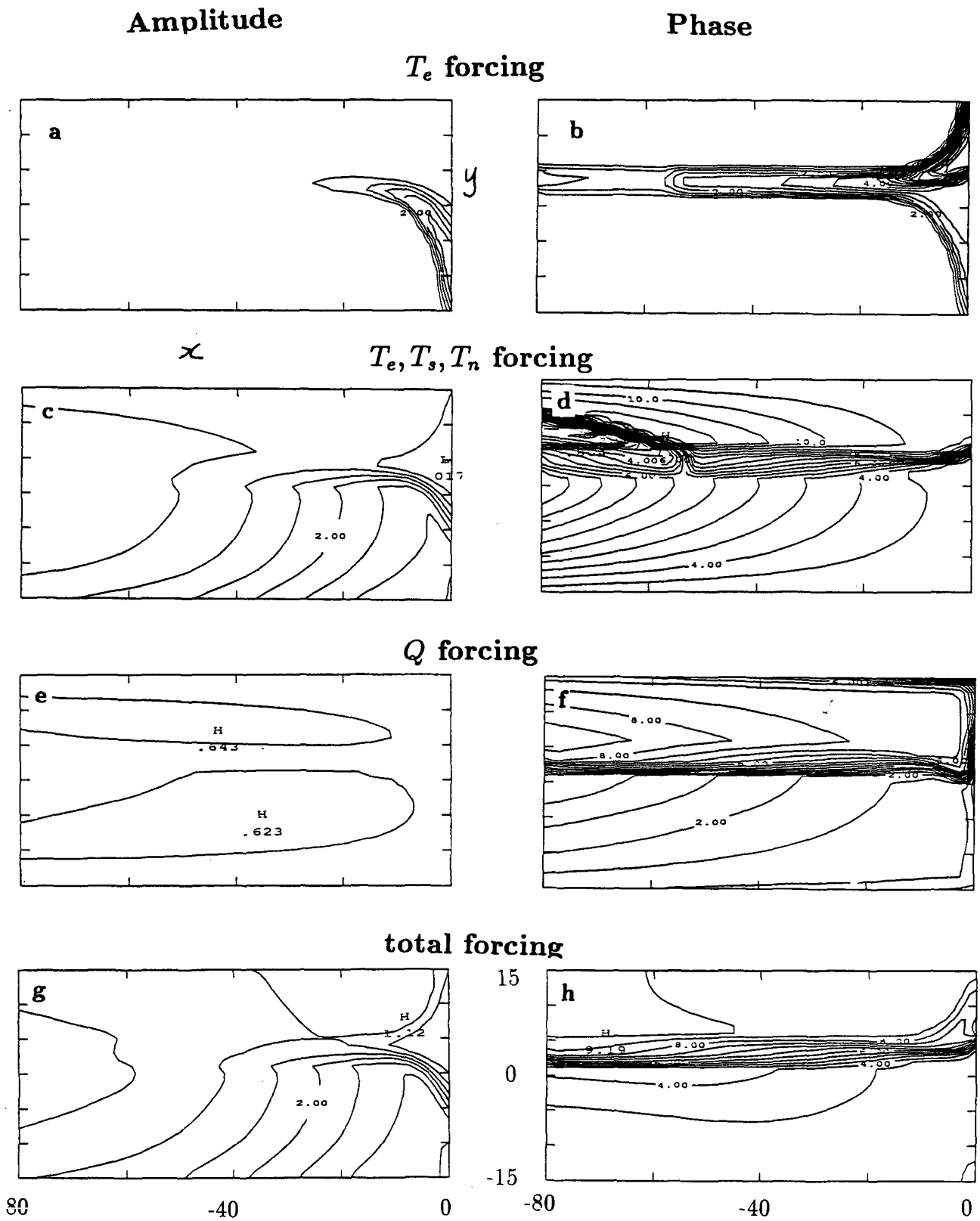

FIG. 8. As in Fig. 6 but for the characteristic field in Fig. 7.

phase propagation. The variability under the total forcing in Figs. 8g,h also shows improvement over the previous case in Figs. 6g,h. For example, in the southwestern part of the domain, the eastward propagation is very slow, similar to the observation in Fig. 1b. As in Fig. 1a, the amplitude exhibits a weak tongue from the northern boundary (0.5° contour), which is poorly produced in Fig. 6g. However, the westward propagation along the equator is still too slow compared with observation. Although some improvement is possible within the context of this model by, say, using a better forcing and mean state, it seems more likely that this deficiency resides in the model physics. We will come back to this point in the final section.

Figure 9 shows the evolution of SST and wind field corresponding to the amplitude and phase in Figs. 8g,h. In January, the eastern Pacific is occupied by cold anomaly centered near the equator. In the middle of February, strong warm anomaly has emerged with a strong gradient of SST anomaly near the equator, which is accompanied by a strong southward anomalous wind component. Through April and May, the warm anomaly south of the equator further expands toward the west and the north.

One unrealistic feature in Fig. 9 is the unrealistically strong meridional wind field. This is related to the strong meridional SST gradient [see (3.1)] produced by the convergence of characteristics as discussed before. Indeed, this can be seen more clearly from the V equation itself. Without zonal variation of the mean wind and SST gradient, the equation for the meridional wind V can be derived directly from the atmospheric and oceanic system (2.1), (2.4), and (2.5) as

$$(\partial_t + K_T)V + (\bar{u} + C_x)\partial_x V + (\bar{v} + C_y)\partial_y V = \frac{\mu}{f^2 + A^2}(A\partial_y - f\partial_x)Q_R - \frac{\beta\lambda_U + A\partial_y\lambda_V}{A(f^2 + A^2)}V,$$

where $\beta = df/dy$, $\lambda_U \sim \bar{U}$, and $\lambda_V \sim \bar{V}$. This equation has the same characteristics as the SST equation in (3.3) except an extra term at the end, which is a damping or growing term (depending on the mean state). Since $\beta > 0$, a westward $\bar{U}$ produces a growing term. Similarly, a $\bar{V}$ field converging toward the equator also contributes to growth. As seen in Figs. 3a,b, these two mean states tend to produce strong convergence of characteristics toward the equator. Since the growth increases along a wave ray, the wind anomaly field intensifies in the converging latitude. As explained above, this strong V component is related to the meridional SST front in the region of converging characteristics.

5. Discussion

An analytical model coupling an atmospheric boundary layer with an oceanic mixed layer is used to study the propagation and evolution of annual variability in the eastern tropical Pacific. It is found that the feedback due to evaporation–entrainment is able to produce a realistic rapid equatorward propagation of coupled annual disturbances from the extratropics. Considering the simplicity of the model, the annual variability of the SST and wind field are produced fairly well over most of the Tropics. The westward propagation, however, seems to be underestimated, particularly in the vicinity of the equator. As a result, the tongue structure of the annual variability is not well simulated near the equator.

The equatorward propagation has been discussed in one extremely simple model; there is evidence that this coupled propagation exists in more complex models. It has been observed that a northwestward propagation with similar features has been observed in an intermediate coupled model (P. Chang 1993, personal communication). In the intermediate model, the atmospheric model is much more complete, albeit linear. It consists of a boundary layer and a two-layer atmosphere (Wang and Li 1993). Thus, the effects of both deep convection and the boundary layer process are considered. The ocean model consists of a full Kraus–Turner model and a subsurface thermocline layer.

In observations, there have been studies showing the possible influence of the extratropical anomaly on the tropical anomaly at interannual timescales. For example, van Loon and Shea (1985) suggested that the anomalous ocean–atmosphere conditions in the southern Pacific south of 15°S may be the precursors for the ENSO events in the eastern Pacific equatorial region in the next year. However, for annual variability, there has been no systematic observational analysis in identifying the propagation of *coupled* ocean–atmosphere disturbances from the extratropics toward the equatorial region. This will be another aspect to be studied in the future.

The simple model results also have some deficiencies. For example, the westward propagation seems to be underestimated, particularly in the vicinity of the equator. As a result, the tongue structure of the annual variability is not well simulated near the equator. These deficiencies may be the result of several factors limiting the capability of the present model, particularly near the equator. First, the crude (and idealized) estimate of the forcing and mean state may contribute partly to the problem. For example, the specified phase in the eastern and southern boundary is less tonguelike than the observation. The neglect of the background "gustiness" in the evaporation term may also affect the sensitivity of the solution.

Most fundamentally, we think, the model dynamics are inadequate, particularly near the equator in the atmosphere. The neglect of "back pressure" in the atmospheric model (2.1) tends to produce a wind and divergence field too strong compared with observation within several degrees of the equator. Therefore, we

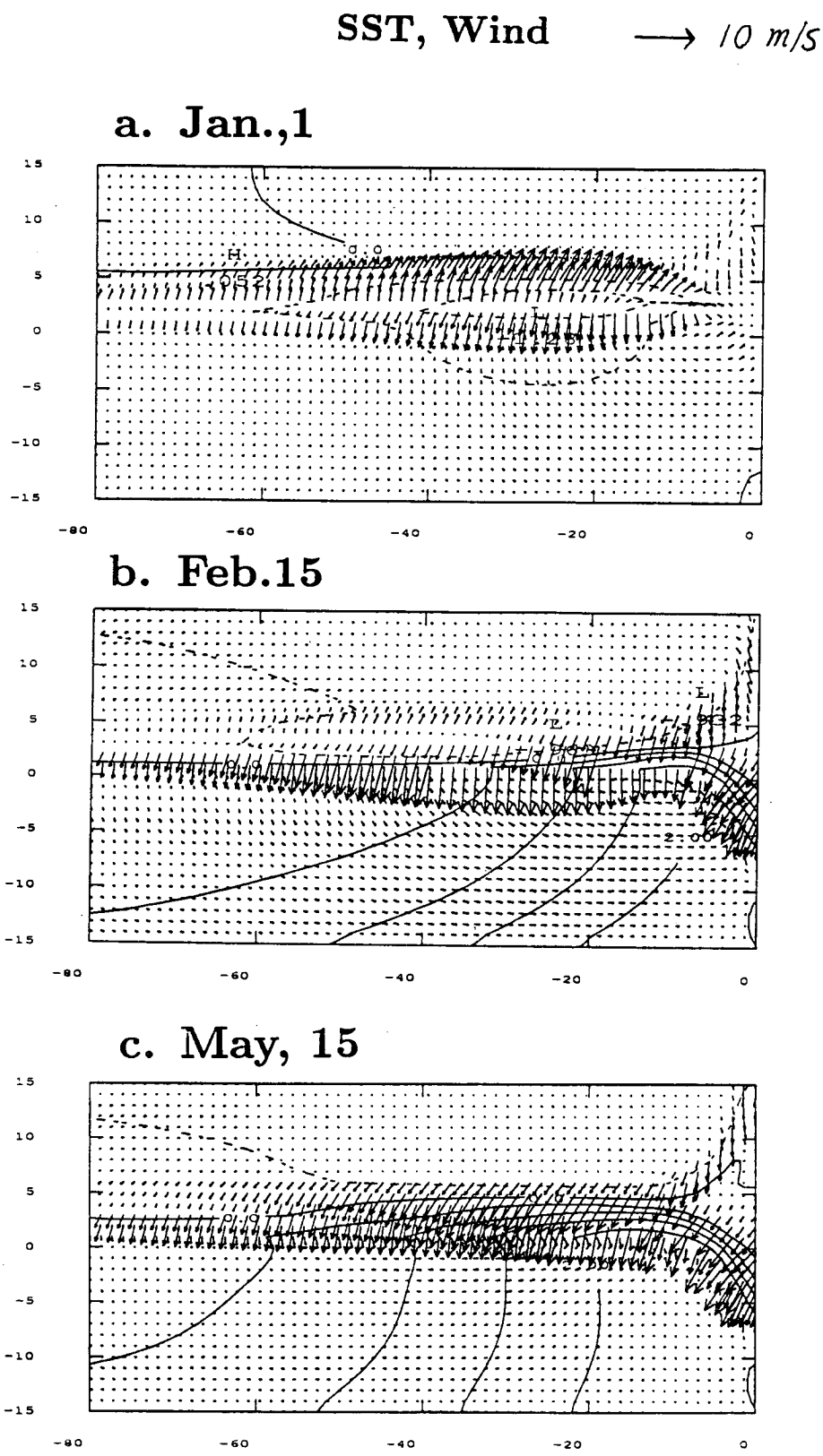

FIG. 9. The evolution of SST (CI: 0.5°C) and surface wind vector anomaly on (a) 1 January, (b) 15 February, and (c) 15 May.

are not surprised to see the relatively poor results on the equator. The next work will be to include the back pressure effect.

If the back pressure effect is included, we will expect the atmosphere to have the capability for a remote response to the extratropics [unlike Eq. (2.1), which depends only on local SST gradient]. One possibility is the response to the remote northern summer monsoon. Mitchell and Wallace (1992) find that the increase in the northward surface winds in response to the onset of the northern summer monsoon may be instrumental in reestablishing the cold tongues in the fall. Therefore, the present model is one extreme case in which the dynamics in both the atmosphere (2.1) and the ocean [(2.5) and also in (2.4) because of the unimportance of the advection] are local, but the coupled system produces a propagation. The remote monsoon effect is the other extreme, in which the atmosphere itself can bridge the extratropics and the equatorial region. The realistic world is likely somewhere in the middle and needs further investigation.

Furthermore, it is also possible that the positive feedback in the equatorial region may also contribute to the annual cycle, especially in the maintaining stage. The recent study of Mitchell and Wallace seems to suggest that the northward wind anomaly and the cold upwelling tend to enhance each other and therefore contribute to the maintenance of the annual cycle in the eastern Pacific and Atlantic. Clearly, further study in both theories and observations is needed.

Acknowledgments. We are deeply indebted to Prof. G. Philander, who introduced to us the problem of equatorial annual variability, and who has shared with us many of his stimulating thoughts and unpublished results. Dr. Ping Chang generously shared with us his unpublished results of a coupled ocean–atmosphere model. Ms. Koeberle produced Fig. 1. ZL also wishes to thank Drs. J. Young and D. Houghton for useful discussions on a revised draft. The comments from two anonymous reviewers were very helpful. ZL was partly supported by a NOAA postdoctoral fellowship on climate change and was partly supported by a Graduate School Research Fund of the University of Wisconsin–Madison. SPX was supported by NOAA Grant NA26G0102-01.

REFERENCES

Anderson, D. L. T., and J. P. McCreary, 1985: Slowly propagating disturbances in a coupled ocean–atmosphere model. *J. Atmos. Sci.*, **42,** 615–629.

Chang, P., and S. G. H. Philander, 1989: Rossby wave packets in baroclinic mean currents. *Deep-Sea Res.*, **36**(1), 17–37.

Gutzler, D. S., and T. M. Wood, 1990: Structure of large-scale convection anomalies over tropical oceans. *J. Climate,* **3,** 483–496.

Hirst, A. C., 1986: Unstable and damped equatorial modes in simple coupled ocean–atmosphere models. *J. Atmos. Sci.,* **43,** 606–630.

Horel, J. D., 1982: On the annual cycle of the tropical Pacific atmosphere and ocean. *Mon. Wea. Rev.,* **110,** 1863–1878.

Kraus, E. B., and J. S. Turner, 1967: A one-dimensional model of the seasonal thermocline. II: The general theory and its consequences. *Tellus,* **19,** 98–109.

Lau, N., G. Philander, and M. Nath, 1992: Simulation of ENSO-like phenomena with a low resolution coupled GCM of global ocean and atmosphere. *J. Climate,* **4,** 284–307.

Lindzen, R., and S. Nigam, 1987: On the role of sea surface temperature gradients in forcing low-level winds and convergence in the tropics. *J. Atmos. Sci.,* **45,** 2440–2458.

Liu, Z., 1993: Penetration of interannual planetary waves across a gyre boundary. *Dyn. Atmos. Oceans,* **17,** 169–186.

McPhaden, J. M., and B. A. Taft, 1988: Dynamics of seasonal and intraseasonal variability in the eastern equatorial Pacific. *J. Phys. Oceanogr.,* **18,** 1713–1732.

Meehl, G. A., 1990: Seasonal cycle forcing of El Niño–Southern Oscillation in a global, coupled ocean–atmosphere GCM. *J. Climate,* **3,** 72–90.

Neelin, J. D., 1991: The slow sea surface temperature mode and the fast-wave limit: Analytic theory for tropical interannual oscillations and experiments in a hybrid coupled model. *J. Atmos. Sci.,* **48,** 584–606.

Philander, S. G. H., and R. C. Pacanowski, 1981: The oceanic response to cross-equatorial winds (with application to coastal upwelling in low latitudes). *Tellus,* **33,** 201–210.

——, T. Yamagata, and R. Pacanowski, 1984: Unstable air–sea interactions in the tropics. *J. Atmos. Sci.,* **41,** 604–613.

Schopf, P. S., D. T. Anderson, and R. Smith, 1981: Beta-dispersion of low frequency Rossby waves. *Dyn. Atmos. Oceans,* **5,** 187–214.

van Loon, H., and D. J. Shea, 1985: The Southern Oscillation. Part IV: The precursors south of 15°S to the extremes of the oscillation. *Mon. Wea. Rev.,* **113,** 2063–2074.

Wallace, J. M., T. P. Mitchell, and C. Deser, 1989: The influence of sea-surface temperature on surface wind in the eastern equatorial Pacific: Seasonal and interannual variability. *J. Climate,* **2,** 1492–1499.

Wang, B., and T. Li, 1993: A simple tropical atmosphere model of relevance to short-term climate variations. *J. Atmos. Sci.,* **50,** 260–284.

Xie, S.-P., A. Kubokawa, and K. Hanawa, 1989: Oscillations with two feedback processes in a coupled ocean–atmosphere model. *J. Climate,* **2,** 946–964.

Yamagata, T., 1985: Stability of a simple air–sea coupled model in the tropics. *Coupled Ocean–Atmosphere Models,* J. Nihoul, Ed., Elsevier, 637–658.